4-15-2008

Spectral Time Moment Analysis of Microgel Structure and Dynamics

Kiril A. Streletzky
Cleveland State University, K.STRELETZKY@csuohio.edu

John T. McKenna
Cleveland State University

Rami Mohieddine
Cleveland State University

Publisher's Statement

This is the accepted version of the following article: Kiril A. Streletzky, John T. McKenna and Rami Mohieddine, "Spectral time moment analysis of microgel structure and dynamics," Journal of Polymer Science Part B: Polymer Physics 46 (8), 771-781 (2008)., which has been published in final form at http://onlinelibrary.wiley.com/doi/10.1002/polb.21406/full

Spectral Time Moment Analysis of Microgel Structure and Dynamics

KIRIL A. STRELETZKY, JOHN T. McKENNA, RAMI MOHIEDDINE

INTRODUCTION

In pursuit of dependable, easy-to-control, submicroscopic, and environmentally sensitive nanoparticles, microgel synthesized from an amphiphilic macromolecule is a promising system with a wide range of applications.[1–6] A good molecule for such system is hydroxypropylcellulose (HPC), which is electrically neutral, water-soluble polysaccharide with a persistence length of about 100.[7,8] HPC is readily available, FDA-approved nontoxic food additive used in soups and ice creams as an emulsifier[9] and encapsulator.[10] Because of its electrical neutrality, semiflexible nature, and solubility in a wide range of solvents, HPC has been widely used for studies of polymer dynamics.[11–24]

As an amphiphilic molecule, HPC undergoes a lyotropic phase transition in aqueous solutions at a critical temperature of $T_c = 41\,^{\circ}C$.[25,26] At low temperatures ($T < T_c$), water acts as a good solvent to polymer chains and HPC forms an isotropic, clear, one-phase system. At high solution temperatures ($T > T_c$), hydrophobic interactions become favorable, water acts as a poor solvent, some linear polymer chains self-associate into poorly soluble, metastable nanoparticles, and the HPC solution separates into two phases with a sudden change first to lucent and then opaque state.[25,27] The phase transition is reversible: cooling HPC solutions below 41 °C brings back the isotropic, clear, one phase system.[25] The co-presence of hydrophobic and hydrophilic regions in HPC molecule allows for

many designs for a controlled self-assembling such as polymeric micelles,[28] a thermally-reversible hydrogel medium,[29] or microgel nanoparticles.[26,30]

Of particular interest are recent findings[26,27] that HPC polymer chains can be chemically crosslinked into stable nanoparticles, called microgels, while they are at solution temperatures $T > T_c$. In solution, these particles may exhibit behavior similar to that of uncrosslinked polymer when water is a good solvent or spherical particles when water is a poor solvent.[30] Under proper conditions (e.g., correct concentration, crosslinking density, etc.) these particles are engineered to undergo a reversible volume-phase transition at T_V, where $T_V \geq T_c$. This transition is due to the hydrophobic–hydrophilic temperature dependence of the HPC polymer chains. At low solution temperatures ($T < T_V$), the microgel will swell due to the absorption of solvent[30,31] and at high temperatures ($T > T_V$) the microgel will expel the solvent due to hydrophobic interactions. The result of this transition is an effective volume *shrinking* of the microgel nanoparticles. A similar transition occurs for bulk, high concentration HPC hydrogel polymers. Microgel nanoparticles, however, undergo much faster response to environmental changes due to their small size.[30] Of course, the important advantage of crosslinked HPC microgels over metastable HPC particles is that microgels are held together both above and below the transition by a crosslinker.

Temperature-sensitive HPC microgel nanoparticles offer a wide range of potential applications from particulate emulsifiers[4,5] and shear-thinning dispersions in coating to permeability modifiers in oil reservoirs[6] and controlled drug delivery and release vesicles in pharmaceutical industry.[3]

In fact, HPC already has many pharmaceutical and clinical applications. The polymer is used as a tablet binder because of its high cohesiveness, binding strength, hardness and low friability.[32] High-viscosity HPC (hydrogel) is used in sustained released matrix applications.[32] HPC is also used as a thickener and stabilizer to maintain and build up viscosity of pharmaceutical liquid.[32] Finally, HPC is used as a bio-adhesive for transmucosal drug administration.[32] The structural and behavioral versatility of HPC microgel particles makes them ideal candidates for application in a variety of targeted drug delivery schemes. They offer many controllable parameters including synthesis techniques, chemical make-up, size, and so forth. These parameters may be adjusted to effectively load medicines into the structure, target diseased tissue (e.g., cancer), and release the payload upon predetermined environmental conditions.

Although synthesis of HPC microgels has been carefully studied,[26,27,31,33] the structure and dynamics of microgels have yet to be meticulously examined. Gao et al.[27] synthesized microgels from polymer-surfactant solutions by inducing phase separation at $T_c = 41$ °C that leads to metastable nanoparticle formation. Metastable HPC formations were then crosslinked into particle-like gel clusters. Xia et al.[26] induced self-association of HPC microgel at ambient conditions without using surfactant, by lowering T_c from 41 to 23 °C with salt addition. Both studies[26,27] used dynamic light scattering (DLS) to characterize the diffusion coefficient and hydrodynamic radius of HPC microgel under the assumption that microgel particles are spheres with a narrow size distribution. Although these assumptions might be acceptable for some microgel systems,[2,3] careful analysis of ref. 27 as well as results of this study (Fig. 1) indicate that microgels synthesized using the recipe of ref. 26 have a wide multimodal size distribution. This finding alludes to the need of independent and self-consistent study of HPC microgel dynamics and structure below and above T_c.

This article presents a study of HPC microgel dynamics in which DLS spectra were analyzed by an alternative approach of spectral line shape and time moment analysis. The next section briefly describes the experimental methods. The third

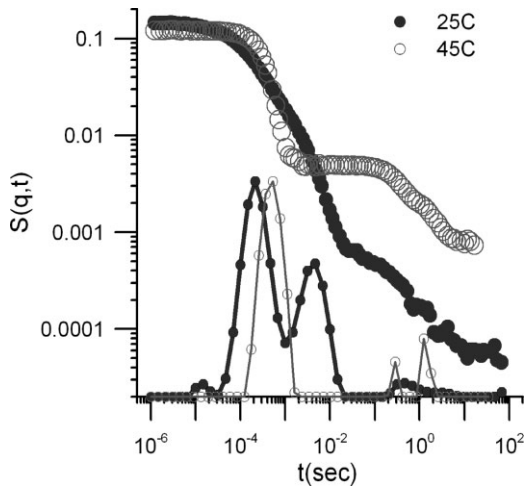

Figure 1. Overlay plot of the measured microgel spectra $S(q,t)$ (open and filled circles) and corresponding decay time distributions (solid lines with open and filled circles) at 25 °C and at 45 °C.

section introduces the basics of spectral line shape and time moment analysis and its application to characterization of complex scattering spectra. The fourth section of the article presents the results on temperature and angular dependences of microgel diffusion. Finally, all the results are brought together in the concluding fifth section.

EXPERIMENTAL

Quasi-elastic light scattering spectroscopy (QELSS) also known as DLS was used to study temporal evolution of concentration fluctuations in aqueous solutions of microgel particles in thermal equilibrium. The intensity of the scattered light $I(q,t)$ was monitored as a function of time and observed light spectrum was recorded as intensity–intensity correlation function $S(q,\tau)$:

$$S(q,\tau) = \int_0^T \mathrm{d}t I(q,t) I(q,t+\tau). \qquad (1)$$

Here q is the magnitude of the scattering vector, $q = \frac{4\pi n}{\lambda} \sin\frac{\theta}{2}$, n is the index of refraction of the medium, λ is the wavelength of light in vacuum, θ is the scattering angle, T is the experiment duration, and τ is the delay time.

In DLS experiments, the laser (Spectra-Physics Stabilite 2017 Ar^+, $\lambda = 514.5$ nm with power output of 1 W) was coupled to a BI 200SM photometer-goniometer (Brookhaven Instruments). Most of the spectra were analyzed by an ALV-5000 correlator while in some cases BI-9000 was used to confirm the results of the ALV size-distribution analysis (CONTIN). Cylindrical glass sample cells (with volume 10 mL), placed into decalin-filled index-matching vat, were maintained at a specific temperature ($23 \le T \le 45$ °C) within 0.1 ° by a Thermo RTE-7 refrigerated bath/circulator. Most experiments were performed at a scattering angle of $\theta = 90$ °($q = 2.30 \times 10^{-2}$ nm^{-1}). The q-dependence of $S(q,\tau)$ was also studied in which goniometer arm was rotated in range of angles $25 \le \theta \le 130$ ° corresponding to the range of the wave vector $7.03 \times 10^{-3} \le q \le 2.94 \times 10^{-2}$ nm^{-1}.

The subject of this study was polymer microgels prepared by crosslinking chains of HPC with nominal molecular weight of 1 MDa ($M_w \approx 855$ kDa[8]) purchased from Scientific Polymer Products. Following the recipe of ref. 26 divinyl sulfone (DVS) from Aldrich was used as a crosslinker. Microgel synthesis was started by first preparing 0.5 wt % stock solution of HPC and 1.44 M salt solution of NaCl. Purified water (resistivity 18 MΩ/cm) from Millipore Milli-Q Academic was used to make all of the stock solutions. In the second step of the synthesis the prepared HPC and NaCl solutions were mixed at $T = 25$ °C in the appropriate amounts to make 0.05 wt % HPC resulting solution. The combined mixture was magnetically stirred until the solution turned light blue and DVS added in the weight proportion of 1 g of HPC to 3 g of DVS. This mixing created a solution with the number of DVS molecules which is 15 times greater than the number of HPC monomers—a proportion that favors the conditions for crosslinking reaction of most (if not all) OH groups of the HPC chains.[26] In the third step of the synthesis, 2 h after crosslinker addition, the small amount (ca. 0.25 g) of 2 M NaOH was added to raise pH of the solution to 12 initiating the crosslinking process. The solution was magnetically stirred during the addition of NaOH and for the next 24 h of the crosslinking process. In the last step, the mixture was dialyzed using cellulose dialysis tybing (with MWCO: 6000–8000) for 5 days to a week to remove NaOH and NaCl. The dialysis process was monitored daily by checking the pH of the solution and replacing the water outside the dialysis tubing with filtered deionized water. Once pH = 7 was reached the dialysis process was terminated. The final solution was filtered through cellulose filters (pore diameter of 1.2 μm) into precleaned and dried sample cells. For comparison purposes the noncrosslinked HPC solution of the same concentration (0.05 wt %) as the resulting HPC microgel solution was also studied. Preparation procedure of the light scattering sample for noncrosslinked HPC was identical to the procedure used with microgel samples.

DATA ANALYSIS

The spectra were analyzed by fitting them to specific functional forms on the level of the field correlation function $g^{(1)}(q,t)$.

A light scattering spectrum (intensity-intensity correlation function) can be expressed via $g^{(1)}(q,t)$, as

$$S(q,t) = A(g^{(1)}(q,t))^2 + B. \qquad (2)$$

where A is the scattering amplitude, determined by various apparatus-dependent factors, and B is the time independent part of the spectrum - the baseline. The nonlinear-least-squares minimization based on simplex algorithm was used to see

which form of $g^{(1)}(q,t)$ describes $S(q,t)$ the best. Each spectrum was fitted repeatedly trying different values of initial parameters and different numbers of modes to determine if the output result has any dependence on the initial guesses and number of parameters. The change was considered insignificant and fit numerically stable if the final output changed by less than 1–2% after the initial guesses were altered.

Spectral relaxations of the $S(q,t)$ span more than seven orders of magnitude in time allowing stable fits to a function with several decay modes. Empirically, the sum of three stretched exponentials was found to be sufficient to describe the field correlation function accurately:

$$g^{(1)}(q,t) = \sum_{i=1}^{N} A_i \exp(-\theta_i t^{\beta_i}). \qquad (3)$$

In this equation, N is the number of modes which are labeled by i; β_i is the stretching parameter; θ_i is the decay pseudorate; and A_i is the mode amplitude. The stretched-exponential form was found to provide an accurate representation of the microgel correlation function when $N = 3$, with β_i and θ_i determining the temporal evolution of each mode. This representation of the $g^{(1)}(q,t)$ is probably not unique but the fits to three stretched exponentials were very reproducible, described the complex shape of the correlation function, and yielded a very small RMS fitting error. A typical normalized spectra and corresponding fits are shown on Figure 2. Three stretched exponentials were used in all fits. The largest RMS error of $\sim 10^{-3}$ among these data set was found at 45 °C for other data sets RMS $\sim 2 \times 10^{-4}$.

The described lineshape analysis approach to highly nonexponential spectra is fundamentally different from a typical Inverse Laplace Transform of $S(q,t)$ used in many DLS algorithms such as CONTIN, in which the distribution of the relaxation rates $A(\Gamma)$ is obtained by inverting the spectra. CONTIN is known to be extremely sensitive to experimental noise,[34] which might lead to misinterpretation of multimodal spectra. Some preliminary experiments were performed both below and above T_c, analyzing the data using BI-CONTIN and ALV-CONTIN programs. The size distribution was found to be multimodal and the output of the both CONTIN programs was found to be very sensitive to algorithm parameters (such range of decays, number of grid points, etc.) and somewhat challenging to reproduce. Although the difficulties with CONTIN analysis can be partially explained

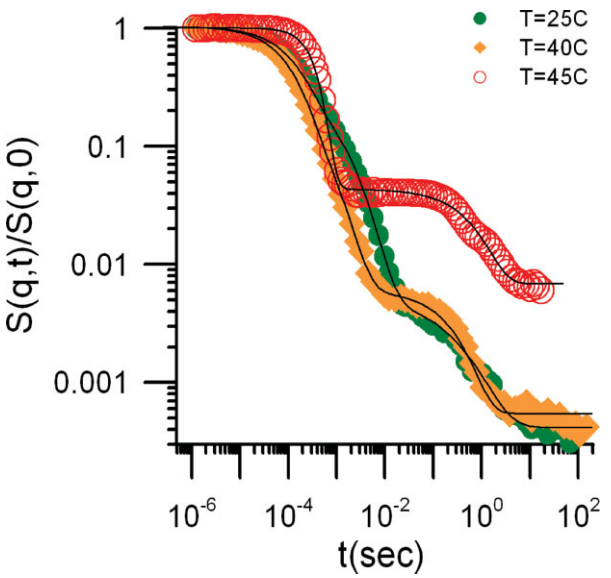

Figure 2. Renormalized spectra $S(q,t)$ of HPC microgels at two solution temperatures below (25 °C and 40 °C) and one solution temperature above the transition (45 °C). Lines shown are fits to three stretched exponentials.

by limited attempts, the robustness and low noise sensitivity of the line shape/time moment analysis[24] were the key factors in choosing the spectral analysis method.

The stretched exponential form used in the line shape analysis provides an accurate while not necessarily unique representation for the field correlation function. To understand the physical properties of the scatterers one can carefully study the behavior of A_i, θ_i, and β_i for each mode as function of scattering angle and temperature as was previously reported for HPC polymer chains[20–23] However, the unattractive feature of this approach is that θ_i, the pseudorate of relaxation, has the dimensions of *time* to a *noninteger* power β_i which is not the same in different spectra and different modes.

As an alternative characterization of light scattering spectra the method of cumulants[35] can be used, which supplies a uniform, convergent, description of any light scattering spectrum in terms of its initial slope and time derivatives. However, for clearly multimodal spectra, an approach that isolates each mode is physically appealing. Here the sum of stretched exponentials was used to characterize the multimodal spectra and the spectral time moments method was employed[24,36] to describe each mode.

The time moments method is based on the fact that any monotonically decaying spectrum can be expanded as a sum of exponentials:

$$g^{(1)}(t) = \int_0^\infty d\Gamma A(\Gamma) \exp(-\Gamma t). \quad (4)$$

Here $A(\Gamma)$ is a normalized decay amplitude associated with decay rate Γ. Typically A is normalized using $\int_0^\infty A(\Gamma)\mathrm{d}\Gamma = 1$.

Spectral time moments M_n come from an extension of the exponential moment integral

$$M_n \equiv \int_0^\infty \mathrm{d}t\ t^n\ \exp(-\Gamma t) = \frac{\gamma(1+n)}{\Gamma^{1+n}}. \quad (5)$$

Here Γ is the true decay rate of a pure exponential; n is the order of the moment M_n, and γ is the Gamma function which should be distinguished from the decay rate Γ. For a pure single-exponential relaxation, $\Gamma = 1/M_0$.

Time moments of $g^{(1)}(t)$ instead of exponential function can be written as

$$M_n \equiv \int_0^\infty \mathrm{d}t\ t^n g^{(1)}(t) = \int_0^\infty \mathrm{d}\Gamma\ A(\Gamma)\frac{\gamma(1+n)}{\Gamma^{1+n}}. \quad (6)$$

Therefore, the time moments are related to decay rates via $M_n/n! \equiv \langle\Gamma^{-n-1}\rangle$ and zeroth time moment M_0 yields mean relaxation time or $\langle\Gamma^{-1}\rangle$.

Time moments M_n are integral averages over $g^{(1)}(t)$. In theory, $g^{(1)}(t)$ has to be measured accurately at long times to determine spectral time moments accurately. Alternatively, the time moments of $g^{(1)}(t)$ can be found by replacing the measured $g^{(1)}(t)$ with its fitting function and integrating it analytically. Analytic integration of one stretched exponential shows

$$M_{0i} \equiv \int_0^\infty \mathrm{d}t \exp(-\theta_i t^{\beta_i}) = \gamma(1+1/\beta_i)/\theta_i^{1/\beta_i}. \quad (7)$$

This approach allows calculation of the mean relaxation time ($\langle\Gamma_i^{-1}\rangle$) of a stretched exponential from its decay pseudorate (θ_i) and stretching exponent (β_i). As was reported earlier,[36] θ_i and β_i are often anticorrelated with respect to experimental noise. However, the integral average that generates the mean relaxation time (M_{0i}) cancels out these correlations, leading to calculated M_{0i} having lower noise than measured θ_i and β_i separately. Since over wide range of times the stretched exponential form is assumed for each mode, the accurate measurements of the field correlation function at shorter times can be used to infer mean relaxation time M_0, without a direct need for perfect measurements of $g^{(1)}(q,t)$ at very large times.

A nominal mean diffusion coefficient corresponding to each mode can be calculated from each mean decay rate, $\langle\Gamma_i^{-1}\rangle$

$$D_i = \langle\Gamma_i\rangle/q^2. \quad (8)$$

In the spectral time moment analysis the properties of each mode are considered to identify physical processes corresponding to a specific mode.

The special case of dilute Brownian spheres in small-molecule, low-viscosity solvents can be described successfully by the Stokes-Einstein equation, which relates the diffusion coefficient of the particle to its hydrodynamic radius R_h and solvent viscosity η

$$D = \frac{k_\mathrm{B}T}{6\pi\eta R_\mathrm{h}}. \quad (9)$$

Here k_B and T are Boltzmann's constant and the absolute temperature. Equation 9 is not valid if the solution is concentrated enough to have the solvent viscosity to be very different from solution viscosity as was theoretically[37] and experimentally[38] shown.

RESULTS AND DISCUSSION

The effect of solution temperature on microgels was studied by repeating 90 ° scattering experiment at various solution temperatures (at the room temperature, 23 °C and at 25, 30, 35, 40, and 45 °C). Above 23 °C the temperature was changed by a step of 5 °C. We waited at least 1 h for the sample to equilibrate by monitoring the count rate. After recording a stable count rate for more than 20 min three or four experiments were performed at a given temperature, each for at least 30 min duration. Since the shrinkage of size distribution is the quintessential property of the microgels, the temperature experiments were also an important test on whether the crosslinking of the polymer chains was successful.

Figure 1 shows the confirmation that we have succeeded in crosslinking polymer chains into a microgel. Indeed, the change in the shape of the correlation function with increasing T is dramatic. At room temperature, the shape of the DLS spectrum shows at least two apparent decays. In addition to very slow process (or processes) at $t \geq 50$ ms, the correlation function at 25 °C reveals multimodal shape at $t \leq 50$ ms. On the other hand, the correlation function measured at 45 °C has unimodal shape at $t \leq 50$ ms with additional slower processes apparent at considerably longer times. Figure 1 also shows the corresponding decay time distributions for two microgel spectra obtained by ALV-CONTIN. Both spectra reveal extremely slow processes at $t \approx 0.2$–3 s that correspond to correlation function plateau and slower decays at $t \geq 50$ ms. More importantly, the correlation functions and corresponding decay time distributions differ significantly at $t \leq 0.2$ s. Microgels at room temperature (25 °C) reveal nonuniform drop and wide bimodal (or trimodal) distribution of decay times ranging between 8 and 20000 μs. The two main peaks of this distribution correspond to a wide multi-modal size distribution ranging from 1 to 3000 nm with two apparent peaks at 25 and 450 nm (not shown). Microgels at 45 °C reveal a steeper drop in correlation function and a considerably narrower unimodal distribution of decay times with $150 \leq t \leq 2000$ μs that corresponds to a size distribution centered at 100 nm and spanning the range from 25 to 350 nm.

The measured correlation functions were reproducible both at high and low T. The apparent volume phase transition of microgels is also reversible: after lowering the temperature from 45 to 25 °C correlation functions with the shape seen before the heating were consistently obtained. If the sample was heated to 45 ° again, the correlation function similar to the one seen at that temperature during the first heating cycle was obtained again. This remarkable reversibility of transition is the key to a fundamental and applied scientific interest in microgels. Corresponding decay time (or size) distribution analysis obtained from microgel spectra using CONTIN revealed some differences. For decay times $t \leq 50$ ms, the narrower decay time distribution at high T was well reproducible, but the wider, multimodal decay time distribution at low T differed somewhat in every experiment. This result together with highly reproducible shape of correlation functions points to a data analysis artifact. The cause for this difference might be twofold. First, CONTIN analysis is very sensitive to the algorithm parameters (such as range of decays, number of grid points, etc.). Special care should be taken in completing a consistent CONTIN analysis of raw data that covers wide range of decay times. This study attempted only approximate CONTIN estimate. Second, there is an intrinsic problem of the CONTIN analysis as indicated by ref. 34 among others. The Inverse Laplace transform, which is the core of the CONTIN algorithm is extremely sensitive to experimental noise. Acquisition times of measured spectra in this study (30–45 min) might have been somewhat short (only 3000–10000 of the longest decay) for accurate measurement of the very slow relaxation processes (at $t \geq 3$ s). Although these slow processes did not affect the lineshape analysis of the rest of the relaxation, they should be taken into account for the proper CONTIN analysis.

To characterize the dynamics of microgel particles (that have relaxation times much shorter than 50 ms) the time moment analysis[24,36] was used. In this analysis, $g^{(1)}(q,t)$ was fit to a sum of three stretched exponentials with 9 parameters according to eq 3. Each of the three modes had an amplitude (parameters A_1, A_2, A_3), a mode width or pseudorate of relaxation (parameters $\theta_1, \theta_2, \theta_3$), and a stretching parameter (β_1, β_2, β_3). Figure 2 shows a few examples of typical fits to the spectrum. Note that the spectra and the fit cover more than three decades of a decay at $T < T_V$.

The resultant parameters of each fit were used to calculate zeroth moment M_{0i} of each mode and, therefore, to obtain a mean relaxation rate $\langle \Gamma_i^{-1} \rangle$ for a particular mode. Figure 3 shows the decays rates of three modes Γ_1, Γ_2, and Γ_3 as a function of temperature. Γ_1 is roughly temperature independent up to 40 °C and has a value of 5–6×10^3 s^{-1}. At 45 °C, Γ_1 drops to 1–$2\times10^3 s^{-1}$. Γ_2, on the other hand, steadily increases from 200 s^{-1} at 23 °C to about 1000 s^{-1} at 45 °C. Notably, $\Gamma_1 \approx \Gamma_2$ at 45 °C, indicating that two modes converge into one. Γ_3 values are scattered especially at lower temperatures. The line on the graph shows a weak trend of increasing Γ_3 with the rise of the temperature from 23 to 45 °C. Similar trends are exhibited by the modes diffusion coefficients (not shown). For $23 \leq T \leq 40$ °C, $D_1 \approx 8$–9×10^{-8} cm^2/s, while D_2 increases from 4×10^{-9} to 10^{-8} cm^2/s as T increases from 23 to 40 °C. At 45 °C, $D_1 \approx D_2 \approx 2$–$4\times10^{-8}$ cm^2/s. D_3 is very scattered slightly increasing on average from 2×10^{-12} to 8×10^{-12} cm^2/s as T rises from 23 to 45 °C.

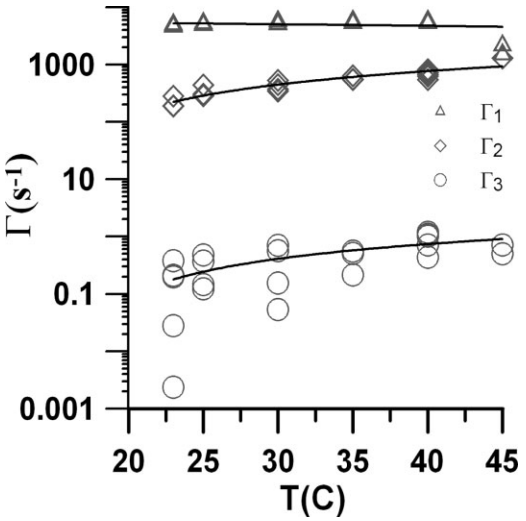

Figure 3. Mean decay rates for three spectral modes of HPC microgel as a function of solution temperature.

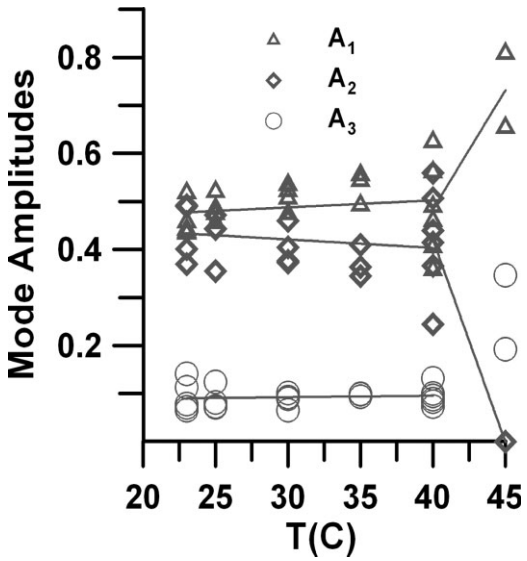

Figure 4. Relative amplitudes of fast (triangles), intermediate (diamonds), and slow (circles) spectral modes of HPC microgel as a function of solution temperature. Lines are drawn to guide the eye.

The graph of mode amplitudes as a function of temperature (Fig. 4) reveals the contribution of specific modes at different temperatures. According to the analysis, modes 1 and 2 dominate at room temperatures (with amplitudes of about 0.4–0.5). Mode 3 contributes only 10–15% at temperatures up to 40 °C. As temperature increases the data becomes slightly more scattered but the main trend is apparent. Above 40 °C the amplitude of mode 1 increases to 0.65–0.75, the amplitude of the mode 2 decreases to about 0, and the amplitude of the mode 3 shows some increase (to 0.2–0.35). In other words, mode 2 completely disappears at 45 °C at the expense of the increase in contributions from modes 1 and 3.

Using Stokes-Einstein Equation (eq 9) the hydrodynamic radius corresponding to each of the modes was calculated. Figure 5 presents R_{h1} and R_{h2} calculated for the first and the second modes respectively. (R_{h3} for the third mode is not shown on Figure 5. On average, $R_{h3} \approx 3$–6×10^{-4} m.) The apparent trend seen on Figure 5 is that modes 2 and 1 (intermediate and fast) combine into one mode at 45 °C. In fact, R_{h1} increases from 25 to 30 nm while R_{h2} decreases from 450–650 nm to 250–300 nm as T changes from 23 to 40 °C. The last heating step from 40 to 45 °C yields merging of the two modes into one mode centered at 100–150 nm.

To facilitate interpretation of the physical meaning of the three modes the angular dependence of microgel light scattering spectra at room temperature (23 °C) was studied. Microgels were studied at a range of scattering angles from 25 to 130 ° corresponding to q-range $7.03 \times 10^{-3} \leq q \leq 2.94 \times 10^{-2}$ nm^{-1}.

Figure 6(a) shows the q-dependence of the mean relaxation rates Γ_1 and Γ_2. Both modes have decay

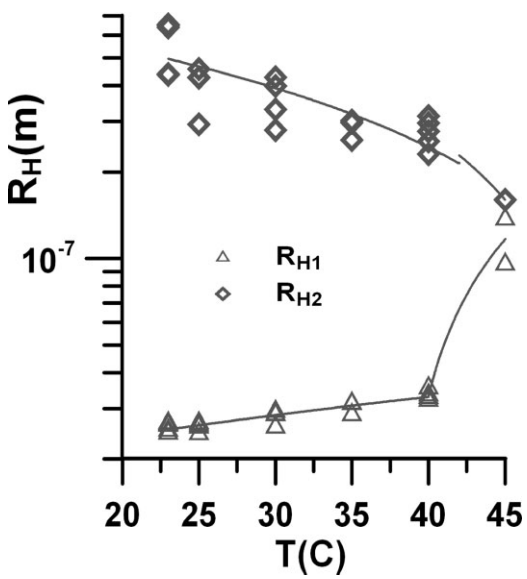

Figure 5. Apparent hydrodynamic radii for the two faster modes from time moment analysis. The fastest mode (triangles) corresponds to $\langle \Gamma_1^{-1} \rangle \approx 5$–$6 \times 10^3$ 1/s at $T \leq 40$ °C. The intermediate mode corresponds to $\langle \Gamma_2^{-1} \rangle \approx 200$–$1000$ 1/s at $T \leq 40$ °C.

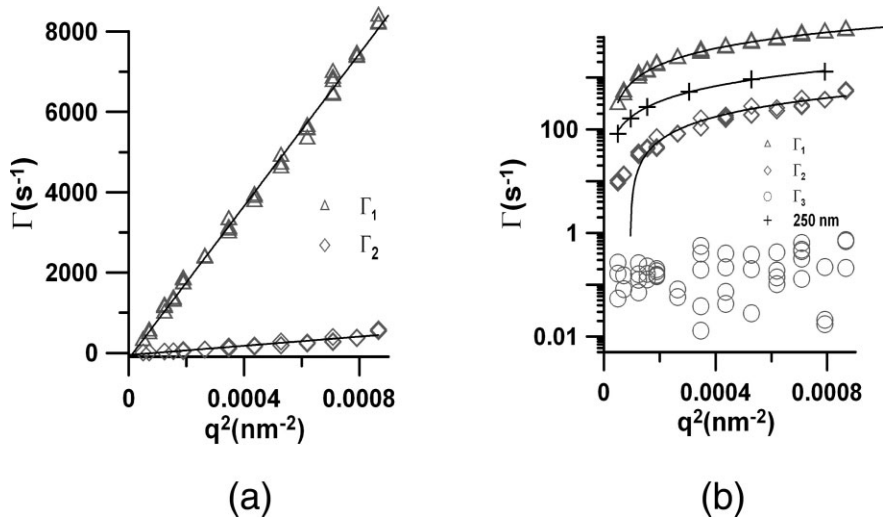

Figure 6. (a) Mean decay rates for the fast (triangles) and intermediate (diamonds) spectral modes of HPC microgel as a function of scattering wave vector squared. Straight lines represent linear fits. (b) Mean decay rates for all three spectral modes on a semi-log plot. The decay rates of $d = 250$ nm latex probes are also shown for a reference. Lines represent the linear fits.

rates that increase linearly with q^2 over most q with very small intercepts at $q = 0$. Figure 6(b), however, shows the same q-dependence on logarithmic scale. It is apparent that q-dependence of Γ_2 diverges from its linear behavior at $q^2 < 0.0002$ nm^{-2}. Figure 6(b) reveals that Γ_3 is fairly independent of q, having a value centered around 0.15 s^{-1}. Figure 6(b) also shows the q-dependence of a decay rate for 250 nm-diameter polystyrene latex probes for comparison. For this control sample, spectra were fitted using eq 3, yielding one dominant pure exponential mode (stretching exponent ≈ 1) and two negligibly small modes (amplitudes $\leq 0.1\%$). Figure 6(b) shows that the latex probes have a purely diffusive behavior with $\Gamma \sim q^2$ and no intercept.

Figure 7 shows corresponding stretching exponents (parameters β_1, β_2, β_3) for the three modes. β_1 and β_2 decrease with increasing q. The q-dependence of β_1 is weaker than the q-dependence of β_2 with $0.85 \leq \beta_1 \leq 1.0$ and $0.65 \leq \beta_2 \leq 1.0$. β_3 is largely independent of q with an average value of 0.3. Figure 7 also compares β_1, β_2, β_3 with two stretching exponents (for sharp and broad polymer modes) obtained by the time moment analysis[39] of noncrosslinked polymer spectra of concentration identical to the one used in microgels (0.05 wt %).

These findings on decay rates and stretching exponents of the three microgel modes suggest that modes 1 and 2 exhibit a diffusive-like behavior. In fact, one can argue that the fastest mode-mode 1 (θ_1, β_1) is more diffusive than the intermediate mode-mode 2 (θ_2, β_2), while the slow mode-mode 3 (θ_3, β_3) shows clearly non-diffusive

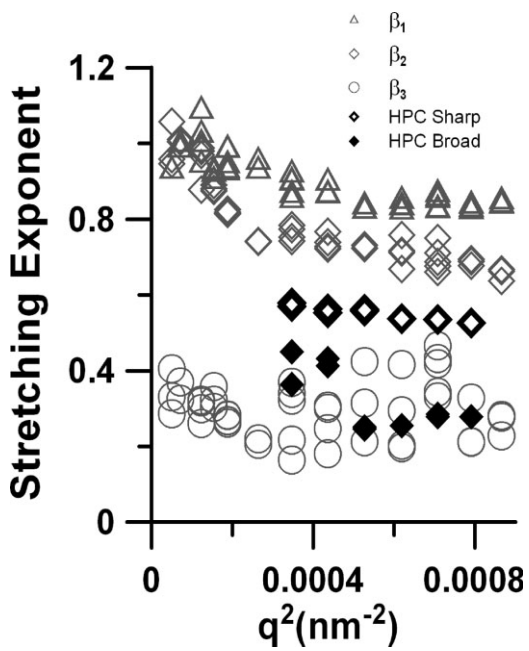

Figure 7. Stretching exponents from time moment analysis for the three spectral modes of HPC microgel as a function of q^2: fast (triangles), intermediate (diamonds), and slow (circles). Small diamonds show the stretching exponents for the two spectral modes (broad and sharp) of noncrosslinked same concentration (0.05 wt %) polymer solution.

behavior reminiscent of linear polymer chain diffusion.

The q-dependence of the amplitudes of the three modes is shown on Figure 8. Clearly at low q, mode 2 is dominant ($A_2 \approx 0.65$–0.7), mode 3 is responsible for about 30% of the spectra, while mode 1 has a very small representation if any ($A_1 < 0.1$). With increasing q, the amplitude of mode 2 decreases to 0.35–0.4, the amplitude of mode 3 also decreases to 0.1, but mode 1 becomes dominant - A_3 increases to about 0.5 at the highest q.

The mean diffusion coefficients obtained for each mode (via eq 8) are shown on Figure 9 as a function of q^2. The fast mode (triangles) yields largely q-independent $D_1 \approx 7$–9×10^{-8} cm^2/s. The intermediate mode (diamonds) yields slightly q-dependent D_2 which changes by a factor of 2–2.5 from 2×10^{-9} to 4–5×10^{-9} cm^2/s with rising q. The slow mode (open circles) reveals D_3 that is centered around 5×10^{-12} cm^2/s. It might be argued that D_3 has a very weak q-dependence, slightly decreasing with an increase of q. Figure 9 also compares the diffusion coefficients of three microgel modes (D_1, D_2, D_3) with the diffusion coefficients obtained for the apparent modes of noncrosslinked polymer of the same concentration (0.05 wt %). The spectra of noncrosslinked polymer were found to be successfully fit to a sum of two stretched exponentials (eq 3) over studied range of q ($1.9 \times 10^{-2} \leq q \leq 2.8 \times 10^{-2}$ nm^{-1}). The

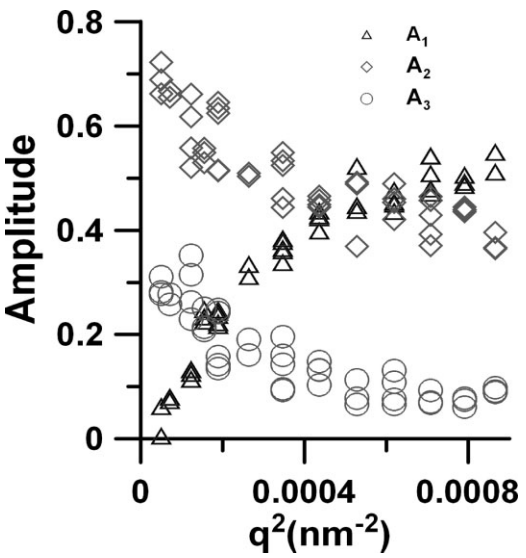

Figure 8. The relative amplitudes of the fast (triangles), intermediate (diamonds), and slow (circles) spectral modes of HPC microgel as a function of q^2.

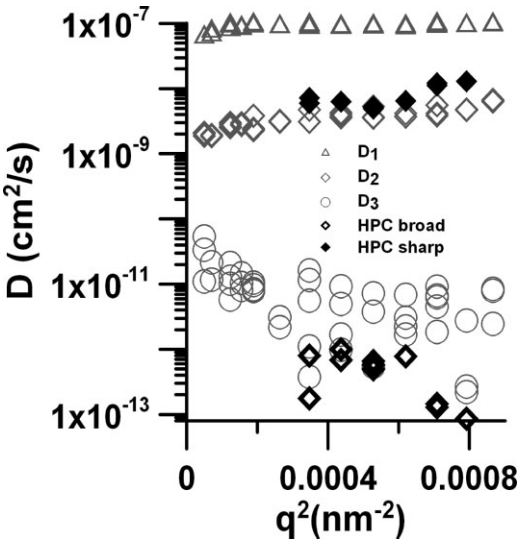

Figure 9. The effective diffusion coefficients $D = \frac{\langle\Gamma\rangle}{q^2}$ for the fast (triangles), intermediate (diamonds), and slow (circles) spectral modes of HPC microgels as a function of q^2. Dark diamonds show the effective diffusion coefficients for the two spectral modes (broad and sharp) of noncrosslinked polymer solution of the same concentration as crosslinked solutions.

open and filled black diamonds on Figure 9 correspond to the two deduced diffusion coefficients of the noncrosslinked polymer, “broad" and “sharp" mode, respectively.[39] The comparison of microgel and polymer diffusion coefficients reveals that: (a) D_{broad} is similar or slightly lower than D_3; (b) D_{sharp} is on average by a factor of two larger than D_2.

The comparison of the effective diffusion coefficients for the microgel modes with the effective diffusion coefficients deduced for the same concentration of noncrosslinked polymer shows that the largest difference between the two systems is the presence of the fast microgel mode in the crosslinked solutions. This mode shows diffusive-like behavior ($\langle\Gamma^{-1}\rangle \sim q^2$ with small intercept, and stretching exponent of ≈ 0.85–1.0) and corresponds to formations with the hydrodynamic radius of 450–650 nm at room temperature. The other two microgel modes have effective diffusion coefficients similar in magnitude to the effective diffusion of the two observed polymer modes. Also, the q-dependences of these microgel and polymer modes are similar: both D_2 and D_{sharp} have similar linear dependence of q^2, while D_3 and D_{broad} are both largely independent of q^2. The similarity, however, is not complete. The broad polymer mode has D_{broad} which is on average by a factor

two larger than the intermediate mode D_2. In addition, the comparison of the stretching exponents (Fig. 7) reveals that while the broad polymer mode has a stretching parameter (0.25–0.4) similar to the stretching exponent of the slow microgel mode (β_3), the sharp polymer mode has a stretching exponent of 0.55–0.6 which is distinctly different from $\beta_2 \approx 0.7$–0.8 of the intermediate microgel mode.

CONCLUSIONS

The results of spectral time moment analysis of the microgel data presented earlier can be summarized as follows:

First, the microgel size distribution and spectral line shape changes drastically upon heating above the volume phase transition temperature T_V. The transition is reversible. The microgels are found to have a wide CONTIN-produced size distribution (or decay time distribution) both below and above T_V. All measured microgel distributions are similar in revealing very slow relaxation processes at $0.2 \leq t \leq 3$ s. However, at $t \leq 50$ ms the distributions below and above T_V are very different. Namely, the distributions are wide and bimodal (multimodal) below the transition and relatively narrow and unimodal above the transition. The line shape analysis reveals the tri-modal spectra at room temperature (below T_V) and bimodal spectra above T_V. Each of the spectral modes is found to be successfully fit to a stretched exponential. In addition, the parameters of the spectral time moment analysis were found to be very reproducible.

Second, the mode composition of the spectra at 90 ° scattering reveals that the main contributors (of about 40–50%) to the spectrum at $T < T_V$ are the fast and intermediate modes with $\Gamma \approx 5000$ and 200–1000 s^{-1} and the stretching exponents of about 0.7 and 0.8, respectively. The third, slow mode, is responsible for only 10% of the spectrum at $T < T_V$. This mode yields somewhat noisy results (due to somewhat short acquisition times for very slow relaxation processes) for Γ centered around 0.2–0.4 s^{-1} and a stretching exponent of about 0.2–0.4.

Third, the temperature increase to $T > T_V$ leads to increase of the fast mode amplitude from 0.45–0.5 to 0.65–0.8, decrease of the intermediate mode amplitude down to zero, and increase in contribution (to 0.2–0.3) of the slow mode. This temperature change also brings merging of the fast and intermediate mode Γ, D, and apparent radii R_H at 45 °C.

Fourth, the angular dependence of the microgel modes reveals that the fast mode has diffusive-like behavior in which $\Gamma \sim q^2$ over the range of angles from 25 to 130 ° with little (if any) intercept. The contribution of this mode drastically increases from 0 to 50% with angle increasing from 25 to 130 °C. The intermediate mode also shows diffusive-like behavior but over the narrower range of angles (50–130 °C). This mode goes from being dominant (amplitude $\approx$ 0.7) at low angles to the one contributing only 40%. The slow mode is largely independent of q, but decreases its contribution from 30 to 10% as the angle changes from 25 to 130 °C.

Fifth, the apparent diffusion coefficients obtained from the time moment spectral line shape analysis for the microgel modes were compared to the apparent diffusion coefficients for the same-concentration noncrosslinked polymer. It was found that below T_V microgel spectra are successfully represented by three spectral modes, while the spectra of noncrosslinked polymer are described well only by two spectral modes. Comparison of the microgel modes with the modes of noncrosslinked polymer revealed that the diffusion coefficients of the two observed polymer modes are similar in values and q-dependences to the diffusion coefficients of the microgel's intermediate and slow modes. However, only the slow mode of microgel has the values of stretching parameter (0.2–0.4) similar to the stretching parameter of one of the two polymer modes (broad mode). The slow microgel mode and the broad polymer mode also have a similar q^2 - dependence of their fitting parameters.[39] The stretching parameters of the microgel intermediate mode and the polymer second mode (sharp mode) are different in values and their q^2 -dependences.

On the basis of the observed T and q-dependences of the microgel modes as well as from the comparison with the results for the noncrosslinked polymer of the same concentration it can be argued that there are two microgel particulate modes, namely the fast and the intermediate modes. The slow microgel mode reveals properties similar to the slow mode observed in noncrosslinked polymer solutions. This mode might represent loose (uncrosslinked) polymer chains. The temperature dependence of the microgel modes is consistent with this picture. Three modes observed below T_V combine into two modes above T_V (see Fig. 4). Indeed, two of the three decay

rates Γ_1 and Γ_2 and corresponding hydrodynamic radii R_{H1} and R_{H2} for the microgel fast and intermediate modes merge at 45 °C (see Figs 3 and 5). These two modes show diffusive-like q-behavior and, therefore, can be interpreted as modes describing particulates. At 25 °C, the observed two modes, representing particulates have very wide size distribution and two main apparent size contributions of 25–30 nm and 450–650 nm. At 45 °C, there is only one mode left with $R_H \approx$ 100–150 nm. This behavior illustrates the shrinkage of the microgel size distribution above T_V. On the other hand, the third mode (the slow microgel mode) does not show the radical change of its parameters above T_V. This microgel mode shows dynamic characteristics of loose polymer chains as can be seen from its q-dependence as well as from the comparison with results on noncrosslinked, same concentration polymer.

The authors thank G. Hillier for experiments on noncrosslinked HPC, G. Phillies for stimulating discussions, and Bryan Carpenter for his help in setting up the DLS lab at CSU. This research was partially supported by the EFFRD AWARD (CSU) and an award from Research Corporation. The support is gratefully acknowledged.

REFERENCES AND NOTES

1. Murray, M. J.; Snowden, M. J. Adv Colloid Interface Sci 1995, 54, 73.
2. Saunders, B. R.; Vincent, B. Adv Colloid Interface Sci 1999, 80, 1.
3. Pelton, R. Adv. Colloid Interface Sci 2000, 85, 1.
4. Langevin, D. Annu Rev Phys Chem 1992, 43, 341.
5. Ngai, T; Behrens, S. H.; Auweter, H. Chem Commun 2005, 331.
6. Snowden, M. J.; Vincent, B; Morgan, J. C. UK Patent, GB 226, 2117A 1993; (b) Li, Y; Liu, Y; Bai, B. Oil Drilling Product Technol, 1999, 21, 3.
7. Aharoni, S. M. Macromolecules 1983, 16, 1722.
8. Mustafa, M; Russo, P. S. J Colloid Interface Sci 1989, 129, 240.
9. Brydon, G.; Ganguly, R.; Ghosh, S. GUT Apr 2003 Supplement, 1, 52, pA9.
10. Watano, S.; Nakamura, H.; Hamada, K.; Wakamatsu, Y.; Tanabe, Y.; Dave, R. N.; Pfeffer, R. Powder Technol 2004, 141, 172.
11. Yang, T.; Jamieson, A. M. J Colloid Interface Sci 1988, 126, 220.
12. Brown, W.; Rymden, R. Macromolecules 1986, 19, 2942.
13. Bu, Z.; Russo, P. S. Macromolecules 1994, 27, 1187.
14. Russo, P. S.; Mustafa, M; Cao, T.; Stephens, L. K. J Colloid Interface Sci 1988, 122, 120.
15. Phillies, G. D. J.; Richardson, C.; Quinlan, C. A.; Ren, S. Z. Macromolecules 1993, 26, 6849.
16. Phillies, G. D. J.; Clomenil, D. Macromolecules 1993, 26, 167.
17. Phillies, G. D. J.; Quinlan, C. A. Macromolecules 1995, 28, 160.
18. Phillies, G. D. J.; LaCroix, M. J Phys Chem B 1997, 101, 39.
19. O'Connell, R. O.; Hanson, H; Phillies, G. D. J. J Polym Sci Part B: Polym Phys 2004, 43, 323.
20. Streletzky, K. A.; Phillies, G. D. J. J Chem Phys 1998, 108, 2975.
21. Streletzky, K. A.; Phillies, G. D. J. J Polym Sci Part B: Polym Phys 1998, B 36, 3087.
22. Streletzky, K. A.; Phillies, G. D. J. Macromolecules 1999, 32, 145.
23. Streletzky, K. A.; Phillies, G. D. J. J Phys Chem 1999, B 103, 1811.
24. Phillies, G. D. J.; O'Connell, R. O.; Whitford, P.; Streletzky, K. A. J Chem Phys 2003, 119, 9903.
25. Mustafa, M. B.; Tipton, D. L.; Barkley, M. D.; Russo, P. S.; Blum, F. D. Macromolecules 1993, 26, 370.
26. Xia, X.; Tang, S.; Lu, X.; Hu, Z. Macromolecules 2003, 36, 3695.
27. Gao, J.; Haidar, G.; Lu, X.; Hu, Z. Macromolecules 2001, 34, 2242.
28. Francis, M.; Piredda, M.; Winnik, F. J Controlled Release 2003, 93, 59.
29. Sinha Roy, D.; Rohera, B. Eur J Pharmaceutical Sci 2002, 16, 193.
30. Lu, X.; Hu, Z.; Gao, J. Macromolecules 2000, 33, 8698.
31. Lu, X.; Hu, Z.; Schwartz, J. Macromolecules 2002, 35, 9164.
32. Guo, J.-H.; Skinner, G. W.; Harcum, W. W.; Barnum, P. E. PSTT 1998, 1, 254.
33. Cai, T.; Hu, Z. Macromolecules 2003, 36, 6559.
34. Phillies, G. D. J. Analyt Chem, 1990, 62, 1049A.
35. Koppel, D. E. J Chem Phys 1972, 57, 4814.
36. Phillies, G. D. J.; Streletzky, K. A. In Soft Condensed Matter: New Research, Dillon, K. Ed., Nova Science: New York, 2007; pp. 219–263.
37. Altenberger, A. R.; Deutch, J. M. J Chem Phys 1973, 59, 894.
38. Phillies, G. D. J.; Streletzky, K. A. Recent Res Dev Phys Chem 2001, 5, 269.
39. Hillier, G. Master Project, Physics Department, Cleveland State University, Spring; 2006.